Process Safety and Environmental Protection 146 (2021) 95–107

Contents lists available at ScienceDirect

Process Safety and Environmental Protection

journal homepage: www.elsevier.com/locate/psep

A 2D CFD model investigation of the impact of obstacles and turbulence model on methane flame propagation

T. Nguyen [a], C. Strebinger [b], G.E. Bogin Jr. [a,*], J. Brune [a]

[a] Colorado School of Mines, United States
[b] Seattle University, United States

ARTICLE INFO

Article history:
Received 16 April 2020
Received in revised form 11 July 2020
Accepted 17 August 2020
Available online 24 August 2020

Keywords:
Obstacle
Methane-air explosion
Turbulence
Flame
CFD modeling

ABSTRACT

The formation of explosive gas zones (EGZs) from flammable vapors, gases, or dust pose safety hazards to many industries. In many cases, explosions may occur in confined areas with obstacles in the path of flame expansion. By studying the effects of obstacle shape, turbulence model, and spark location on flame propagation and turbulence, a more complete understanding of the flame and fluid dynamics interaction has been achieved. Reynolds Averaged Navier-Stokes (RANS) models were tested to determine if these simplified turbulence models could capture the flame dynamics and propagation velocities using fewer computational resources compared to the higher fidelity Large Eddy Simulation (LES) turbulence model. Results showed that square obstacles caused faster flame propagation compared to hexagons and circles. The square had an average flame propagation velocity 26 % faster than the circle, and the hexagon was 16 % faster than the circle using a k-ω model. Modeling results indicate variation of spark location by as small as 10 % of the obstacle diameter can result in a difference of the flame propagation. Findings on turbulence model accuracy and computational time along with shape comparison can be applied in future modeling of large systems, providing crucial information for safety planning and explosion prevention.

1. Introduction

Methane-air explosions pose safety hazards to various industries, including oil and gas, agriculture, chemical, and coal mining where methane is emitted in the process. Explosive gas zones (EGZs) can form from gas sources including natural gas wells, coal, or the digestive byproducts of livestock. An ignition in the EGZ may be caused by something as small as a static charge to friction caused by falling rocks. The Occupational Safety and Health Administration (OSHA) states that a variety of materials, equipment, or operations can be an ignition source if it can emit a spark or flame, ranging from static electricity to grinding operations and catalytic converters (The Occupational Safety and Health Administration, 2019). In many cases, explosions occur in confined areas with various obstacles obstructing the flame propagation.

Chemical, mining, and petroleum are some of the industries where methane and other chemical explosions pose a threat. In the Jiangsu province in China, smaller industrial accidents are not uncommon, but a recent explosion at the Tianjiayi Chemical Co. on March 21st, 2019, killed 78 people and injured more than 600. The explosion caused shock waves which traveled over 3 km and broke windows, and the resulting flames spread to adjacent buildings (Barrett, 2019; Shih, 2019). Methane explosions are also possible in livestock facilities in the case of poor ventilation in confined areas, which cause an accumulation of methane from manure. Small ignitions from motors or even pilot lights can set off a flash-over or explosion (Chambers et al., 2013). In the Piper Alpha oil platform explosion on July 6th, 1988, which resulted in 135 casualties, an accumulation of methane clathrate in the pipe system caused a build-up of pressure and resulted in an explosion (Cullen, 1990). Since the oil rig also included a gas conversion process for companies Tartan and Claymore, the explosion was worsened since gas production was unable to be immediately stopped. Fires were also enlarged by an explosion from one of Tartan's gas lines, which caused over 16.5 tons per second of gas to feed into Piper Alpha (Liley, 2013). In an underground longwall coal mining process, methane emanating from the coal bed is diluted with ventilation air circulated through the mine by large fans. Under certain conditions, ventilation air mixing with methane can form EGZs that accumulate in the production area, the "face," as well as the mined-out area, the "gob" (Brune and Saki, 2017; Juganda et al., 2017; Wang et al., 2014). In the 2010 Upper Big Branch mine explosion that killed 29 miners, investigators concluded that methane migrated from the gob

* Corresponding author at: Colorado School of Mines, 1610 Illinois St., Golden, CO, 80401, United States.
E-mail address: gbogin@mines.edu (G.E. Bogin Jr.).

https://doi.org/10.1016/j.psep.2020.08.023
0957-5820/

into the face where it formed an EGZ that ignited when the mining machine, the shearer, cut sandstone rock in the "roof" above the coal bed. The initial methane explosion ignited a subsequent coal dust explosion that propagated through 68 km of underground mine workings (Mine Safety and Health Administration., 2010; Brune, 2014).

Since industrial explosions often occur in enclosed spaces such as buildings and mines, the resulting flame interacts with obstacles, whether that be production equipment, plant infrastructure, or buildings. Due to the large scale of industrial explosions along with the wide range of systems where an explosion is possible, it is difficult to predict how the explosion will behave. Computational fluid dynamics (CFD) modeling of an ignition in a large-scale system can provide insight into explosion behavior for major hazard assessments and result in safer design and engineering controls that prevent injury and equipment damage. A major challenge in simulating an explosion within a confined space is determining how to model the flame interactions with obstacles.

The work presented investigates the accuracy and computation efficiency of various RANS and LES turbulence models that could be applied to a combustion model, as well as the effects of obstacle shape on flame propagation. The motivation for this work is to understand the flame interactions with rock rubble in the gob and the impact of the ignition location within or near the gob. To fundamentally understand both impacts, a simplified model for stoichiometric methane flame propagation was developed. Researchers investigated the impact of the obstacle shape, accuracy of RANS versus LES turbulence models, and effects of ignition location relative to the obstacle. Prior research has shown that increasing blockage ratio (Masri et al., 2012; Park et al., 2007; Na'inna et al., 2014; Chen et al., 2016; Li et al., 2017; Zipf et al., 2013; Kindracki et al., 2007; Moen et al., 1982) and the quantity of obstacles (Moen et al., 1982; Li et al., 2018a) both tend to increase the flame propagation velocity. Researchers also investigated other factors that may impact the flame by maintaining a constant blockage ratio for a single obstacle. By modeling flame propagation over a single obstacle, researchers can make a more informed decision on which shape to use to model obstructions in a confined system.

2. Background

2.1. Turbulence

If an ignition were to occur in a confined space with various obstacles, such as the gob of a longwall mine, it is expected that the flow will become turbulent rather than laminar. Turbulence is an important factor that can drastically impact the behavior of flames and how they spread. With a highly turbulent flow, the flame front is expected to wrinkle and stretch, increasing the surface area and thus, the temperature and rate of combustion. If strain from the velocity field causes the flame to stretch, the flame may tear and cause localized quenching, preventing complete combustion from occurring (Turns, 2012; Law, 1989). Other researchers have observed that the introduction of an obstacle to a flow significantly increases the turbulence, so selection of an appropriate turbulence model is crucial (Wen et al., 2012; Ibrahim et al., 2009; Li et al., 2018b; Moen et al., 1980). With increased computing power over the years, using a Large Eddy Simulation (LES) model has become more feasible and thus more common, but a simpler Reynolds Averaged Navier-Stokes (RANS) model may still provide reasonable accuracy with less computational resources. Choosing a turbulence model that minimizes computational time while maintaining solution accuracy will allow researchers to produce larger scale models at reasonable computation times.

There are three main types of turbulence models commonly used in CFD modeling: Direct Numerical Simulations (DNS), Large Eddy Simulations (LES), and Momentum Models. Despite DNS being the most detailed, it is also the most computationally intensive as it resolves all scales of motion (Moin and Mahesh, 1998; Hawkes et al., 2005). LES solves spatially filtered versions of governing equations where only large-scale flows are solved directly while smaller scales are modeled, often with one of several sub-grid scale (SGS) models. The spatially filtered Navier-Stokes equation used by the LES turbulence model, shown as Eq. 1, filters out eddies whose scales are smaller than the filter width used in the computations (ANSYS, Inc., 2013). The left-hand side of Eq. 1 is the continuity equation which shows how the velocity field changes as a function of time (the first term) and space (second term). The right-hand side of Eq. 1 represents the pressure gradient (second term of right-hand side) and normal and shear stress effects (first and third term of the right-hand side).

$$\frac{\partial}{\partial t}\left(\rho\bar{u}_i\right)+\frac{\partial}{\partial x_j}\left(\rho\bar{u}_i\bar{u}_j\right)=\frac{\partial}{\partial x_j}\left(\sigma_{ij}\right)-\frac{\partial\bar{P}}{\partial x_i}-\frac{\partial\tau_{ij}}{\partial x_j} \tag{1}$$

The Smagorinsky-Lilly model is the simplest and most commonly used as it can produce reasonable results for a wide range of flows; the dynamic version of the model is able to update the Smagorinsky constant based on resolved scales of motion (ANSYS, Inc., 2013). While the Wall-Adapting Local Eddy-viscosity (WALE) sub-grid scale model is better able to handle wall bounded flows, the Smagorinsky-Lilly is able to handle flows with unstructured numerical methods and without homogeneity, which is expected of a highly turbulent flow seen in this case (Nicoud and Ducros, 1999). Moment models solve equations for lower-order statistical moments; RANS models are first-order single-order moment closure equations while Reynolds Stress Models (RSM) are second-moment closure. Two-equation RANS models, which includes k-ω, standard k-ε, realizable k-ε, and RNG k-ε, are more common. The main differences between most two-equation models lie in the empirical wall-damping functions and the model constants (Bailly and Comte-Bellot, 2015). Turbulent viscosity of the k-ε turbulence model uses Eq. 2 while the k-ω model uses Eq. 3, where k is the turbulent kinetic energy (J), ε is rate of dissipation (m^2/s^3), C_μ is a constant, α^* is damping coefficient, and ω is specific dissipation rate (s^{-1}) (ANSYS, Inc., 2013). Turbulent kinetic energy increases with velocity of the fluid while the rate of dissipation is the breakdown of eddies. As the large eddies break down, turbulent kinetic energy is cascaded down from large eddies to the smaller ones. Turbulent kinetic energy is dominant at the larger scale, but at the small scale, viscous forces become dominant. If turbulent viscosity increases, shearing and heating of the fluid also increases.

$$\mu_t=\rho C_\mu\frac{k^2}{\varepsilon} \tag{2}$$

$$\mu_t=\alpha^*\frac{\rho k}{\omega} \tag{3}$$

The k-ε model is able to handle shear flows but has difficulty with flows with adverse pressure gradients and separation. Developments in the k-ω model have allowed for higher accuracy in solving the boundary layer and effects of the adverse pressure gradient (Argyropoulos and Markatos, 2015; Kuo and Acharya, 2012).

2.2. Modeling flame interaction with obstacles

Past experiments have investigated the effect of blockage ratio and the shape of obstacles, but not many have modeled a single obstacle in detail by varying the turbulence model or spark location due to the complexities of modeling turbulent flame interaction with solid surfaces (Wen et al., 2012; Ibrahim et al., 2009; Moen

et al., 1980; Na'inna et al., 2017). Masri et al. (2000) found that obstacles with square cross sections had the fastest flame propagation velocities in an experiment with a single obstacle in a vertical combustion chamber (Masri et al., 2000). In addition to the obstacle shape, increasing the blockage ratio also increased flame propagation velocity (Park et al., 2007; Masri et al., 2000). Modeling of the experiment by Masri et al. (2000) has also been done by Kirkpatrick et al. (2003) with an in-house code, developed by Kirkpatrick called PUFFIN, using the Large Eddy Simulation (LES) turbulence model with a Smagorinsky-Lilly subgrid scale (SGS) model (Masri et al., 2000; Kirkpatrick et al., 2003; Ranga Dinesh et al., 2013). Di Sarli et al. (2009) has used an LES model to study the increase in overpressure caused by an obstacle of three different shapes, blockage ratios, and three different fuel equivalence ratios (Di Sarli et al., 2009). Rather than modifying PUFFIN or developing our own in-house code, the commercial software, ANSYS Fluent 17, was used due to ease of use and to reduce development time of a new model.

By using a commercial software, the model will be readily available to those in need of a combustion model that may be used for design and mitigation plans along with many other applications. An experiment conducted by Chen et al. (2016) also paired results with a CFD model using ANSYS Fluent (Chen et al., 2016). Instead of a vertical combustion model with the obstacle centered in the chamber to allow two paths or the flame to travel, Chen et al. (2016) used a horizontally oriented chamber with the obstacle placed on the bottom where the flame could only pass over the obstacle; varying blockage ratio was tested but not the shape of the obstacle. Chen et al. found that increasing the blockage ratio will increase the flame propagation velocity. ANSYS Fluent (version 6.3.26) has also been used to model a vertically oriented combustion chamber in the model by DiSarli et al. (2009) (Di Sarli et al., 2009). DiSarli et al. found that sharp-edged obstacles compared to round-edged obstacles increase flame reactivity.

The turbulence model is important when determining how obstacle shape impacts flame propagation. Previous models by Ibrahim et al. (2009), Kirkpatrick et al. (2003), and Chen et al. (2016) used an LES turbulence model but used a flame surface density SGS instead of a 2-step methane-air reaction to model the chemistry like the model to be presented in this paper (Chen et al., 2016; Ibrahim et al., 2009; Kirkpatrick et al., 2003). Modeling results by Prasad et al. (1999) shows that the flame profiles are significantly different based on which flame surface density (FSD) model is used, even when flow parameters and initial and boundary conditions are the same due to constants in the production and destruction rate equations (Prasad and Gore, 1999). Using the 2-step methane-air reaction rather than the FSD limits model sensitivity to initial conditions. While most models consider chemical reactions with a transport equation using a progress variable (Li et al., 2018a; Ibrahim et al., 2009; Kirkpatrick et al., 2003; Ranga Dinesh et al., 2013; Di Sarli et al., 2009; Boger et al., 1998), the model discussed in this paper uses a simplified 2-step methane-air reaction. When modeling the reactions using a progress variable, the transport equation is reliant on equations for conservation of mass, momentum, and energy; the scalar terms in these equations are also reliant on whether the flame is premixed and its equivalence ratio (Bray et al., 2005). The 2-step equation used in this model uses an Arrhenius rate equation, with constants determined from experimental results, to model the reaction (Dryer and Glassman, 1973). By using the Arrhenius rate equation, the model will be more flexible to changing variables.

3. Combustion model setup

3.1. Geometry

Numerical and experimental results from Masri et al. (2000) and Kirkpatrick et al. (2003) are used as an initial reference to build the 2D model [35, [36]. Results from Masri et al. (2000) and Kirkpatrick et al. (2003) are being used as Masri et al. have continued to further investigate the effect of obstacle arrangement impact on flame propagation while Kirkpatrick's PUFFIN model has been used and referenced in other experiments and LES modeling of turbulence interaction with obstacles, such as Ibrahim et al. (2009) and Ranga Dinesh et al. (2013) [24, [37]. A 0.195 × 0.745 m 2D vertical solution domain was created with the center of the obstacle located 0.15 m from the bottom. The original experimental combustion chamber was 0.545 m in height, but 0.2 m was added in the model to fully capture the flame behavior towards the open end. Obstacles were centered 0.15 m from the bottom, and the ignition location was centered 2.5 cm from the bottom. Fig. 1 shows a diagram of the model along with dimensions used in the 2D model.

3.2. Spark model

The ignition was modeled with an ANSYS Fluent (version 17.0) Spark Model; parameters of the spark model are shown in Table 1. The initial kernel radius was chosen as 2 mm as it was an average between initial radii of numerical cases (4 mm for Ibrahim

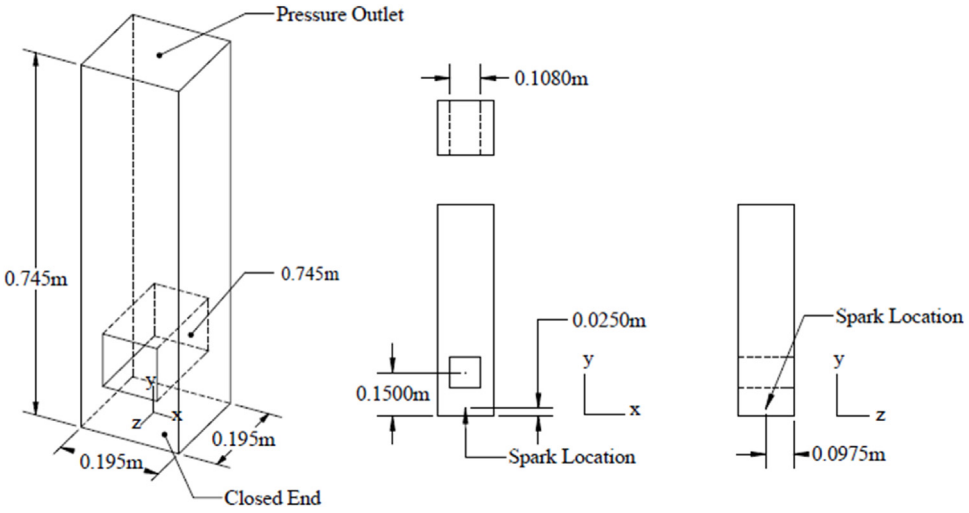

Fig. 1. Diagram of solution domain in 3D. 2D model is of the XY plane with gravity acting in negative y-direction. Origin is along the chamber axis.

Table 1
Parameters of ANSYS Fluent Spark Model used to initiate combustion.

Spark X, Y, Z Coordinates	(0,0.025,0)m
Spark Start Time	0s
Spark Duration	1 ms
Ignition Energy	60 mJ
Kernel Expansion Model	Laminar
Initial Kernel Radius	0.002 m

Table 2
Modeling methods of properties in the methane-air 2-step mixture.

Property	Modeling Method
Mixture Species	Names
Reaction	Finite-rate
Mechanism	Reaction-mechs
Density [kg/m^3]	Ideal-gas
Cp (Specific Heat) [J/kg-K]	Mixing-law
Thermal Conductivity [W/m-K]	Ideal-gas-mixing-law
Viscosity [kg/m–s]	Ideal-gas-mixing-law
Mass Diffusivity [m^2/s]	Kinetic-theory
Thermal Diffusion Coefficient [kg/m–s]	Kinetic-theory
Laminar Flame Speed [m/s]	Metghalchi-keck-law

et al. (2008), 5 mm for Di Sarli et al. (2009), and 3 mm for Li et al. (2018)) and the spark gap of common spark plugs, used in experimental results by Masri et al. (2000), which may average anywhere between 0.4–1.7 mm (Ibrahim et al., 2009; Li et al., 2018b; Masri et al., 2000; Di Sarli et al., 2009). Other papers have referred to their spark location as an ignition with no specification (Na'inna et al. (2016), Li et al. (2018), and Masri et al. (2000)), but what as will be discussed later, the spark location will impact the shape of the flame (Li et al., 2018a; Na'inna et al., 2017; Masri et al., 2000).

3.3. Species transport model

A species transport model was used with a methane-air two step reaction. Parameters of the species model included volumetric reactions, a stiff chemistry solver, diffusion energy source, full multicomponent diffusion, and thermal diffusion. Modeling methods of properties in the methane-air 2-step mixture are listed in Table 2. Direct use of finite-rate kinetics with no turbulence-chemistry interaction was used. Values for the Arrhenius rate equation, Eq. 4, came from experimental results from F.L. Dryer and I. Glassman (1973) (Dryer and Glassman, 1973). Values list in Table 3 are those used in ANSYS Fluent where the reaction order has already been factored in and units have been converted. Species in the model was initialized at stoichiometric conditions and velocity components were zero for a mixture at rest.

$$k = AT^b e^{-\frac{E_a}{RT}} \quad (4)$$

3.4. Boundary conditions and solver settings

Boundary conditions included a 0-gauge pressure outlet at the top opening while the chamber walls, closed end, and obstacle were set as adiabatic no-slip walls. A transient pressure-based solver with gravity as -9.8 m/s^2 in the y-direction was selected. The fluid body was set with the methane-air 2 step reaction and initialized with a stoichiometric methane-air mixture at rest with a temperature of 293 K and operating pressure of 101 kPa. Spatial discretization of the model used second order upwind for all parameters except for momentum, which used a bounded central differencing method. Pressure-velocity coupling was modeled with a PISO scheme and time integration used a bounded second order implicit formulation.

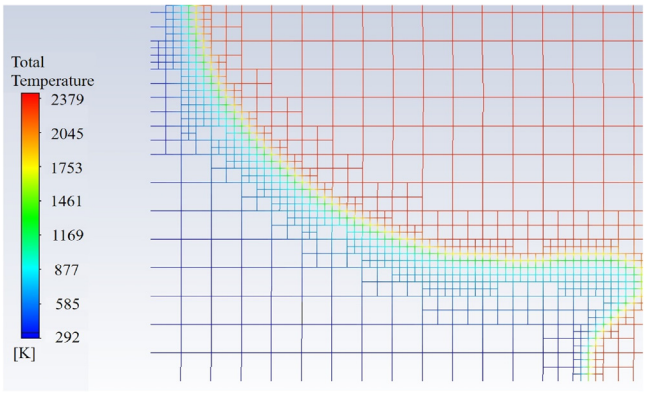

Fig. 2. Mesh of case with a 2 mm base mesh and temperature adaption on the temperature gradient with 2 levels.

Convergence was achieved by ensuring all residuals dropped at least three magnitudes at every timestep. Each timestep size was 1×10^{-5} seconds and was allowed to reach a maximum of 350 iterations, convergence was eventually reached before 350 iterations as more timesteps progressed. The residual criteria were set to 1×10^{-5} for continuity, x-velocity, and y-velocity, 1×10^{-6} for energy, and 1×10^{-4} for turbulence and species parameters. Other turbulence models tested also used the same convergence criteria where the turbulence parameters (k, ω, ε…) were set to 1×10^{-4} to achieve convergence.

3.5. Meshing

Mesh independence was determined by using CO mass fraction, total temperature, and flame front location. The percent difference of the three variables evaluated are shown in Table 4 while the final mesh independent sizing for each turbulence model is shown in Table 5. Each zone had a uniform mesh with no edge sizing or inflation layers. Mesh adaptation by two levels was also added on the temperature gradient to further refine the flame front. As shown in Fig. 2, mesh adaptation on the temperature gradient with two levels allows for 4–10 cells to be at the flame front.

4. Results and discussion

4.1. Shape comparison

Various obstacle shapes were investigated to determine which could be a simplified model for rocks within the gob. Three different shaped obstacles were investigated in the 2D model for shape comparison: a circle, hexagon, and square cross section with dimensions shown in Table 6. These shapes were chosen for simplicity to capture flame interaction with geometric features such as sharp corners or curved surfaces which may be present in obsta-

Table 3
Arrhenius rate reaction equation coefficients for methane-air two step reaction (Dryer and Glassman, 1973).

Reaction	A [kmol/m^3]	Temperature Exponent, b	E_a [J/kg · mol]	Reaction Order
$CH_4 + 1.5O_2 \longrightarrow CO + 2H_2O$	5.012×10^{11}	0	2×10^8	$[CH_4]^{0.7}[O_2]^{0.8}$
$CO + 0.5O_2 \longrightarrow CO_2$	2.239×10^{12}	0	1.7×10^8	$[CO][O_2]^{0.25}[H_2O]^{0.5}$

Table 4
Percent difference of three variables used to determine mesh independence for k-ω and LES turbulence models.

Turbulence Model	Mesh Comparison	CO Mass Fraction [%]	Total Temp [%]	Flame Front Location [%]
k-ω	4 mm v. 2 mm	54	22	7
	2 mm v. 1 mm	6	3	6
LES	2 mm v. 1 mm	15	7	13
	1 mm v. 0.5 mm	6	3	11

Table 5
Mesh sizing for mesh independent solution for each turbulence model used in the investigation. The corresponding fluid zone is shown in Fig. 3.

Turbulence Model	Zone 1 Mesh [mm]	Zone 2 Mesh [mm]
k-ω	2	2
k-ε	2	2
SST	2	2
LES	0.5	1

Table 6
Dimensions and shapes of modeled obstacles for shape comparison.

Shape	Blockage Ratio [%]	Hydraulic Diameter [m]	Side Length [m]
Circle	55	0.063	–
Hexagon	55	0.036	0.054
Square	55	0.108	0.108
Square	41	0.079	0.079

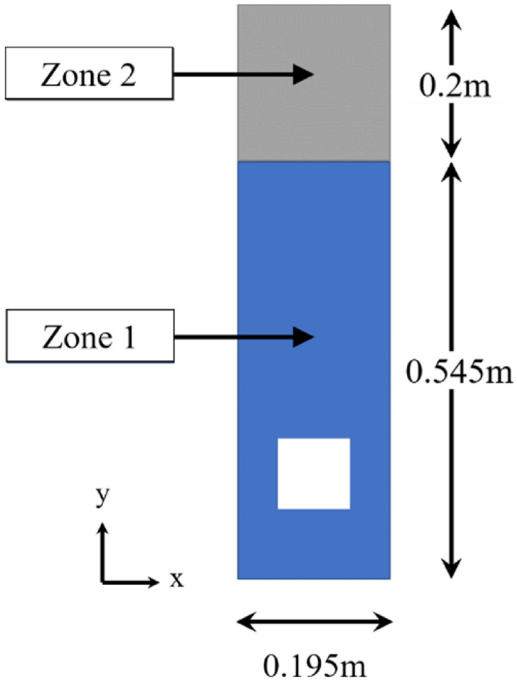

Fig. 3. Diagram of mesh sizing of 2D single obstacle geometry.

cles of more complex shapes. A blockage ratio of 55 % was chosen to match the experiment of Masri et al. (2000) for model validation of shape comparison trends (Masri et al., 2000). The square with a smaller blockage ratio of 41 % rather than 55 % was tested to compare the model with results from Kirkpatrick et al. (2003) which used methane unlike Masri et al. (2000) which used liquefied petroleum gas (LPG) (Kirkpatrick et al., 2003).

4.1.1. Results using the k-ω turbulence model

Results show the square cross section has the greatest flame propagation velocity, flow separation, and formation of vortices. From Fig. 3, it is seen that introducing an obstacle to the flow increases the flame propagation velocity and that the shape of the

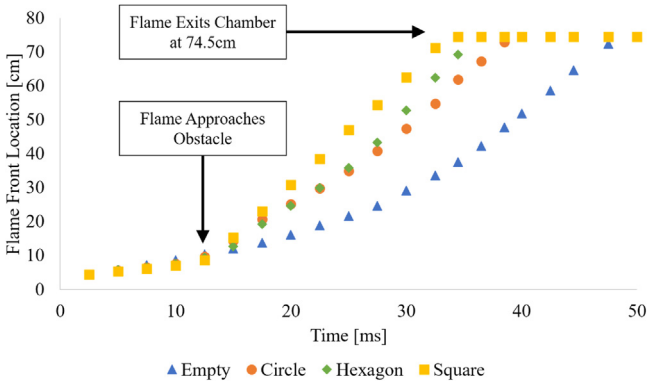

Fig. 4. Flame front location as a function of time for 2D k-ω turbulence model without an obstacle and with a square, circle, and hexagon obstacle. Flame begins to approach obstacle at 12.5 ms for all three obstacles. Temperature =293 K, Pressure = 101 kPa, E_{ign} = 60 mJ, Spark duration =1 ms.

obstacle also has an impact. Various methods can be used for tracking the flame front location, including tracking the OH radicals, location of highest temperature gradient, and reaction rates (Masri et al., 2012, 2000; de Goey et al., 2005). In the results presented here, the flame front is defined as the highest location where the temperature is 2200 K. Flame propagation velocity was calculated from the slope between the flame front location point at which the flame impinges on the obstacle to the last point of each data set (Fig. 4).

The average flame propagation velocity increased from 15.3 m/s with no obstacle to 18.9 m/s with the circle, an increase in velocity by 24 %; the hexagon increased the velocity by 37 % and the square by 42 %, relative to the case with no obstacle. Compared to the case with no obstacle in the flow, the average acceleration increased by 21 % for the circle, 69 % for the hexagon, and 105 % for the square. The trend where the shape of the obstacle has limited impact on the flame propagation during early stages of expansion agrees to the experimental results seen by Masri et al. (2000) and Yu et al., 2016). All three obstacles showed pockets of unburnt methane gas, shown as the black contour in Fig. 5; it is clear that areas of unburnt gas were more present with a square cross section. The circle and hexagon obstacles showed behaviors of vortex shedding with alternating eddies in the wake zone, also seen by Masri et al. (2000). Vortex shedding could cause vibrations in the gob as fluid moves to fill in the low-pressure zones caused by the alternating eddies. The square cross section, on the other hand, has more vortices and flow separation in the wake zone, causing more of the methane to be unburned as the flame progresses forward.

With the formation of boundary layers, it becomes more difficult to burn all the methane as the flame progresses. Shown in Fig. 5, a square obstacle has much more unburnt methane due to vortices which are formed directly behind the obstacle. CFD results from Kirkpatrick et al. (2003) also show formation of vortices in the same locations with smaller vortices at the leading corners of the square and larger ones behind the square in the wake along with the same flame propagation shape (Kirkpatrick et al., 2003). For the square, the mixture continues to burn even after the flame has exited the chamber since there is still a large quantity of unburnt

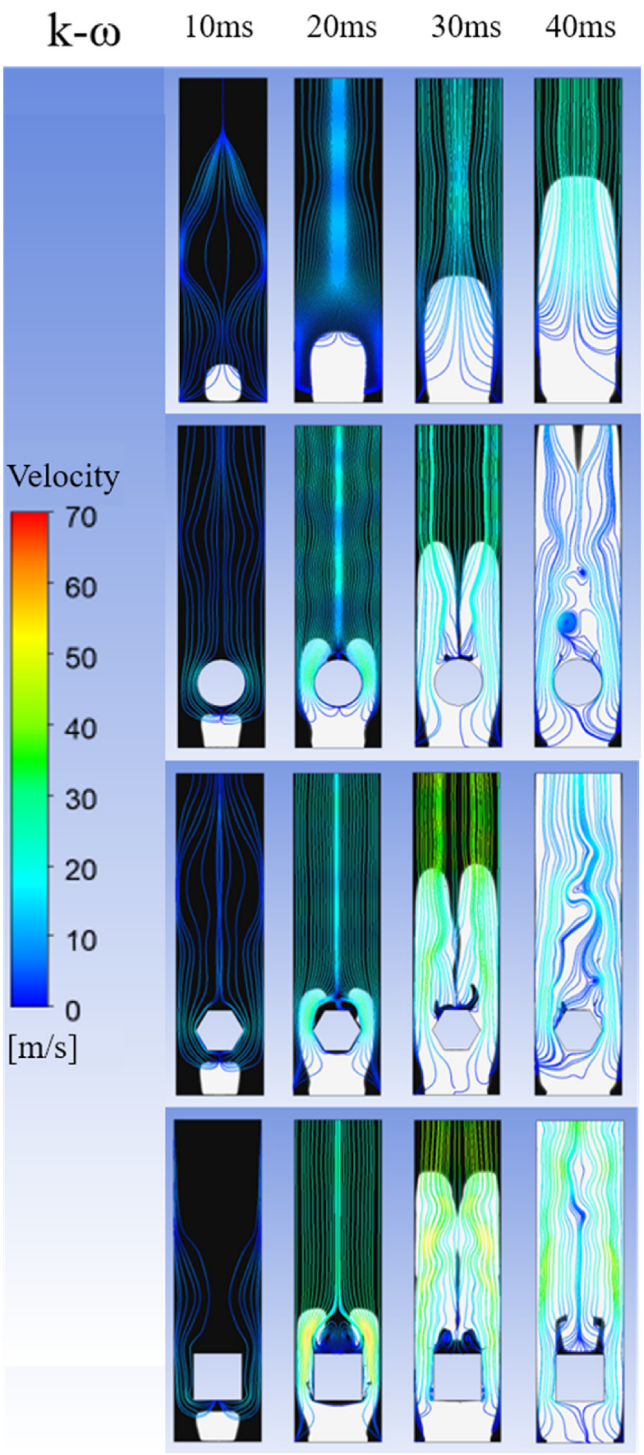

Fig. 5. Flame propagation for 2D k-ω turbulence model. Black contour represents unburnt methane while white contour represents products. Spark location at 2.5 cm centered from bottom with opening at top. Temperature =293 K, Pressure = 101 kPa, E_{ign} = 60 mJ, Spark duration =1 ms.

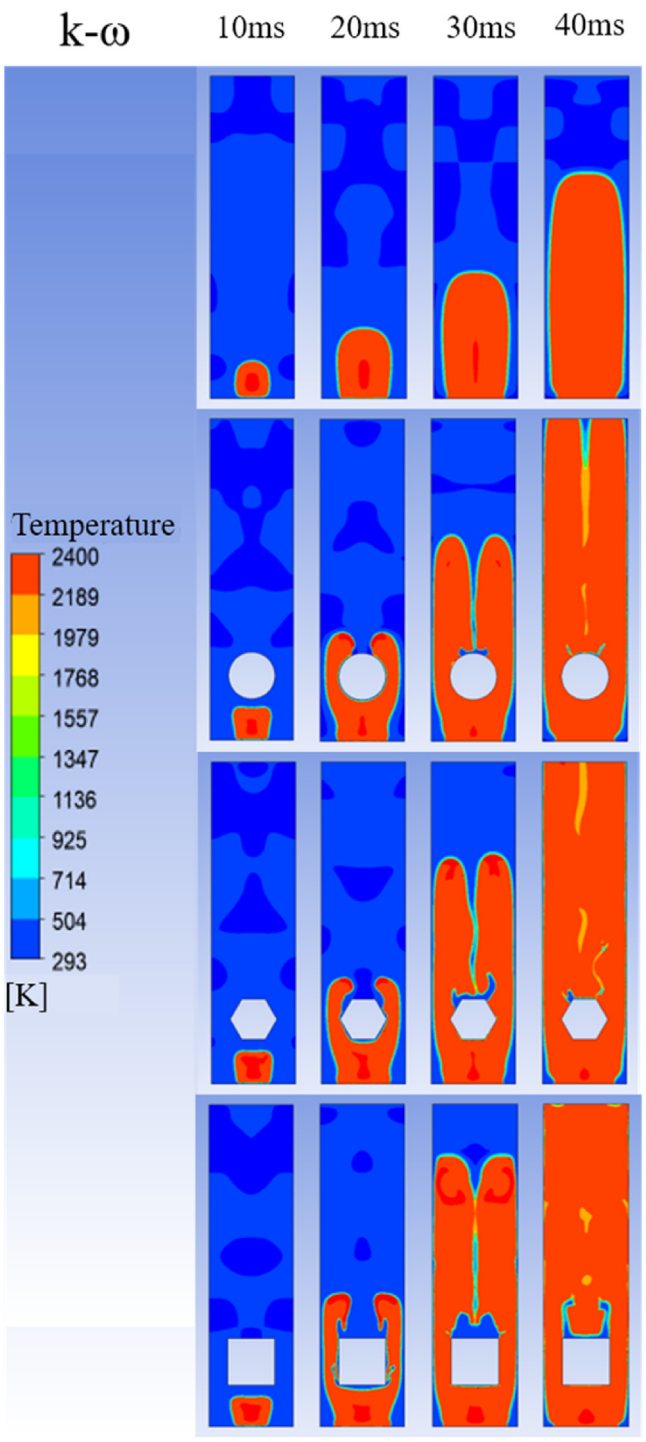

Fig. 6. Temperature contour to show flame propagation for 2D k-ω turbulence model. Spark location at 2.5 cm centered from bottom with opening at top. Temperature =293 K, Pressure = 101 kPa, E_{ign} = 60 mJ, Spark duration =1 ms.

methane, showing that there may be incomplete combustion. The k-ω model showed temperatures around 2300 K within the flame, falling within expected temperature ranges for methane-air combustion, seen in Fig. 6. Obstacle shape was found to have a negligible impact on the temperature of the flame. The slightly elevated average temperature is potentially due to the model only being in 2D, and using a 2-step chemistry does not allow for dissociation.

4.1.2. Results using the LES turbulence model

Major differences between the k-ω and LES model (using a Smagorinsky-Lilly sub-grid scale model) are increased wrinkling of the flame front and flame propagation speeds. The methane contour and streamlines in Fig. 7 and temperature contour in Fig. 8 show that the flame front is not as smooth as the k-ω model. The LES model captures more local variations in species concentrations, temperature, and velocity near the flame front that result in local accelerations. This effect is more apparent with the square obstacle. The velocity streamlines also show that higher velocities occur

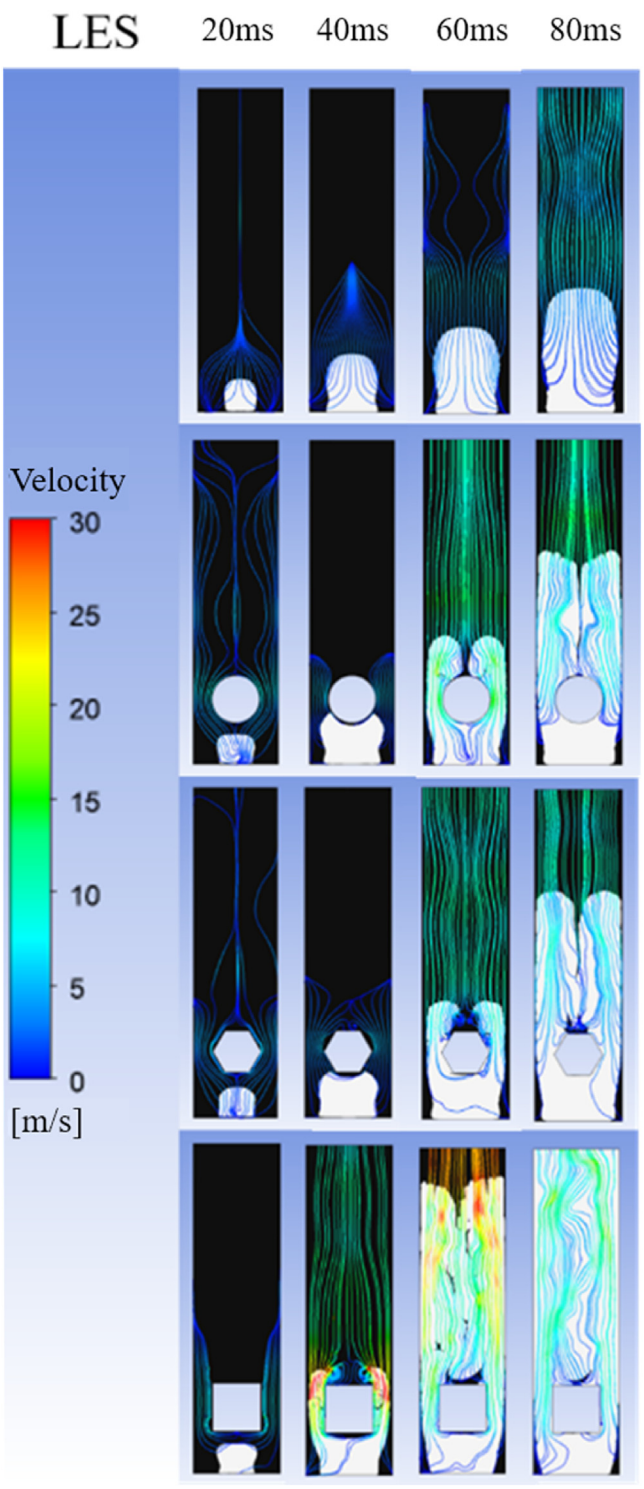

Fig. 7. Flame propagation for 2D LES turbulence model. Black contour represents unburnt methane while white contour represents products. Spark location at 2.5 cm centered from bottom with opening at top. Temperature =293 K, Pressure = 101 kPa, E_{ign} = 60 mJ, Spark duration =1 ms.

towards the flame front and in areas where there are more eddies as expected. Compared to the k-ω model, the LES model captured similar behavior of small pockets of unburnt methane behind the obstacle after the flame passed and in the bottom corners of the chamber. Similar to the k-ω model, the LES model also showed average temperatures around 2300 K within the flame. Obstacle shape also had negligible effect on the flame temperature. Like the k-ω model, the square obstacle in the LES model had the fastest flame propagation (12 m/s) with a flame propagation velocity increase of 219 %, 84 %, and 103 % compared to the empty case, circle, and hexagon, respectively. Fig. 9 shows that, with the LES model, the flame passing the square obstacle reached the end of the chamber twice as fast as with the hexagonal and circular obstacles. Results by Masri et al. (2000) also showed that the circular obstacle had the slowest flame acceleration past the obstacle due to faster flame reattachment, causing a shorter duration of higher turbulence combustion (Masri et al., 2000). Since the size of the circulation zone and vortices behind the obstacle play an important role in flame

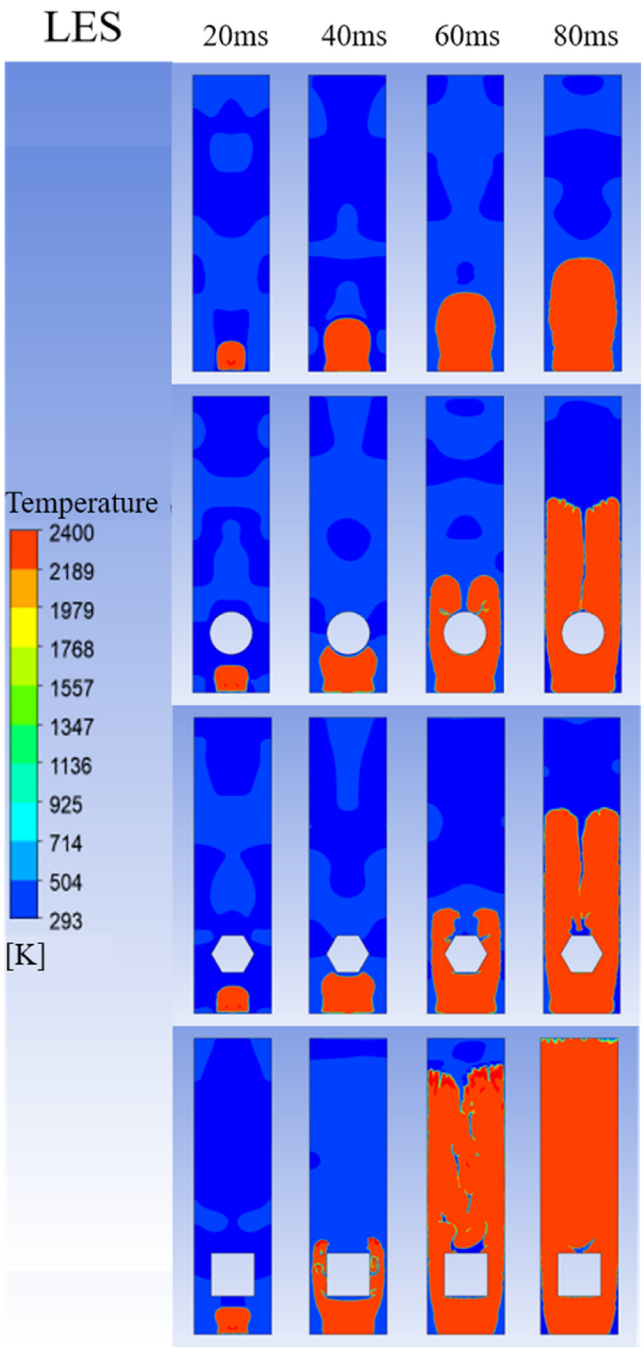

Fig. 8. Temperature contour to show flame propagation for 2D LES turbulence model. Spark location at 2.5 cm centered from bottom with opening at top. Temperature =293 K, Pressure = 101 kPa, E_{ign} = 60 mJ, Spark duration =1 ms.

stretching and propagation, the ability of a turbulence model to predict flame propagation past obstacles will be dependent on its ability to resolve turbulent eddies. It is possible that the LES model resulted in a greater difference between the flame propagation of the square obstacle compared to the circle and hexagon because it was able to resolve the large eddies more accurately than the k-ω model.

Greater wrinkling of the flame increases the surface area of the flame front, thus increasing the combustion rate. Kinetic rate of the methane reaction for the empty scenario and the three obstacles are shown at 60 ms in Fig. 10. It is seen that the three cases with an obstacle have a large surface area for the flame front; this is caused by the eddies stretching and bending the flame front compared to it being fully smooth. At 60 ms, the maximum reaction rate of methane is 4567, 5160, 6092, and 7626 mol/m^{3}s for the empty, circle, hexagon, and square obstacle, respectively. As seen with the velocity streamlines in Fig. 7, the square obstacle creates the most mixing of the fluid out of the four cases as more eddies are formed, followed by the hexagon and circle obstacle, and then the empty case. The three cases with an obstacle also have methane reacting behind the flame front, shown in the light blue and red contour scattered inside the primary flame front outline. Reactions occurring after the flame front has passed is due to eddies that may have trapped pockets of unburnt methane as the flame front passed by and are then reacting later.

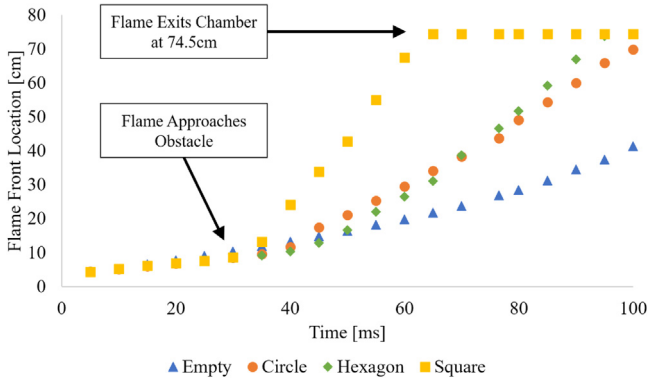

Fig. 9. Flame front location as a function of time for 2D LES turbulence model without an obstacle and with a square, circle, and hexagon obstacle. Flame begins to approach obstacle at 30 ms for all three obstacles. Temperature =293 K, Pressure = 101 kPa, E_{ign} = 60 mJ, Spark duration =1 ms.

4.2. Turbulence model comparisons

Fig. 11 compares velocity streamlines and methane concentrations for the four turbulence models at the same flame front location. The LES turbulence model showed flame wrinkling on the flame front, unlike the k-ω model, which showed a smoother flame front. These differences are more visible when comparing temperature contours of the flames further down the flow; see Fig. 6 for the k-ω model and Fig. 8 for the LES model. Flame wrinkling is a concern since the flame now has a greater surface area, increasing the combustion rate, potentially resulting in increased temperatures and increased propagation velocities. The SST and k-ε model showed similar flame shapes as the k-ω where the flame front was smooth.

Flame thickness for each turbulence model was calculated based on the temperature gradient when the flame front was 38 cm from the bottom of the chamber. The flame thickness was calculated using Eq. 5, which has also been used to calculate flame thickness by Lafay et al. (2007) and de Goey et al. (2004) (de Goey et al., 2005; Lafay et al., 2008).

$$\delta = \frac{T_b - T_u}{\frac{dT}{dx}\Big|_{max}} \tag{5}$$

Results from Fig. 12 show that the LES turbulence model had the smallest flame thickness at the leading flame front with a thickness of 2 mm. The SST, k-ω, and k-ε turbulence models followed with 3, 3, and 8 mm, respectively. When the flame thickness was measured vertical centerline, the flame thickness decreased by 25–50 % except for the case of the SST turbulence model where there

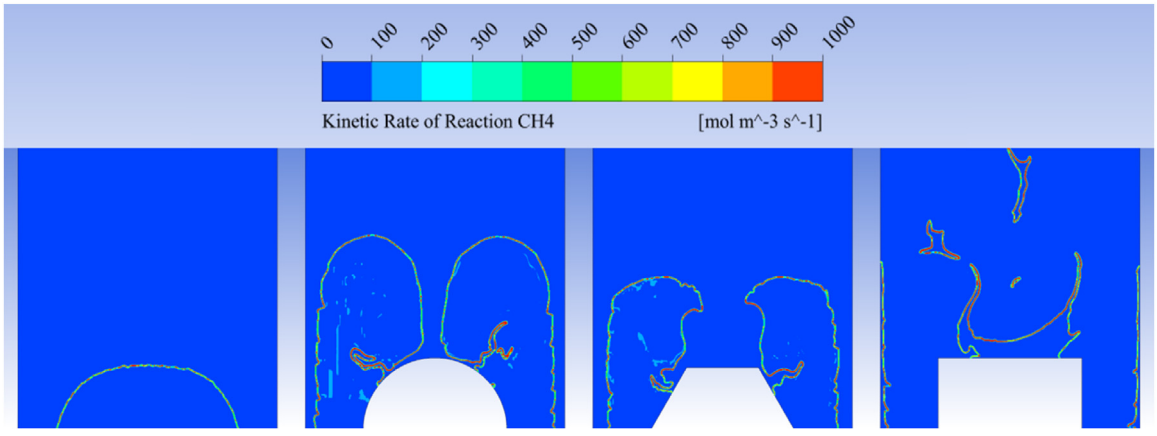

Fig. 10. Kinetic rate of reaction of methane for the four obstacle cases at 60 ms with the LES turbulence model. Images are a close up of Fig. 7 and Fig. 8 at the 60 ms case.

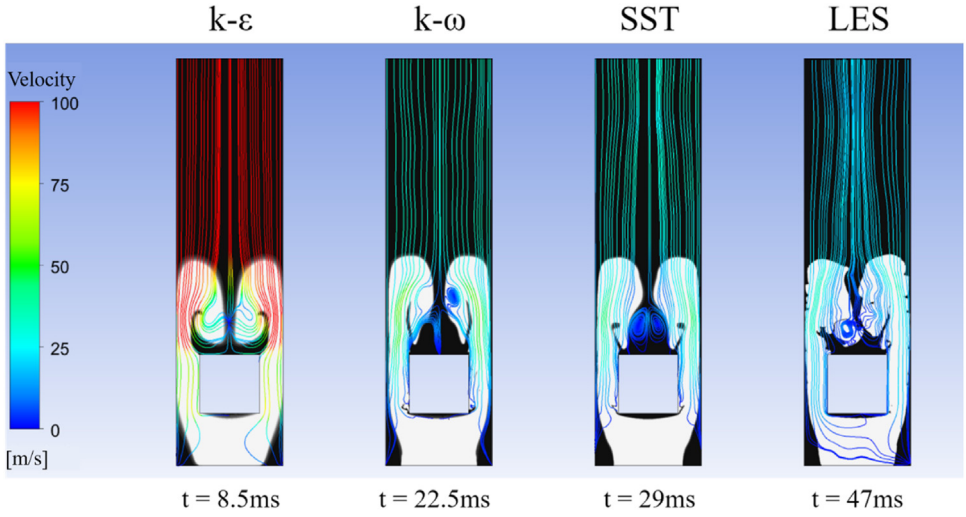

Fig. 11. 2D model with various turbulence models with the flame front at 38 cm from the bottom of the chamber. Black contour represents unburnt methane while white contour represents products. Spark location at 2.5 cm centered from bottom with opening at top. RANS model used 2 mm mesh size. LES model used 0.5 and 1 mm mesh size. All cases initialized with a stoichiometric mixture. Temperature =293 K, Pressure = 101 kPa, E_{ign} = 60 mJ, Spark duration =1 ms.

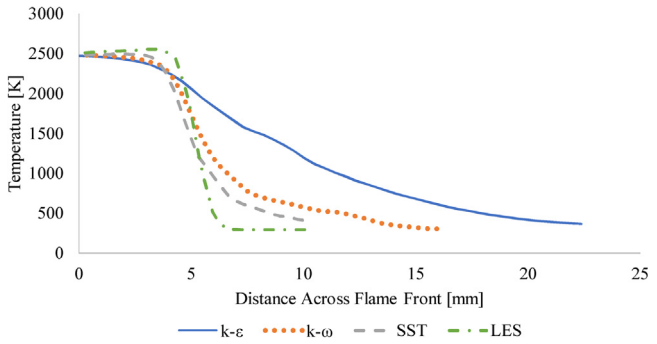

Fig. 12. Temperature across flame front for four turbulence models with the square obstacle. The four cases are were all when the flame was 38 cm up the chamber. Temperature data was taken in the y-direction through the leading flame front with 100 points.

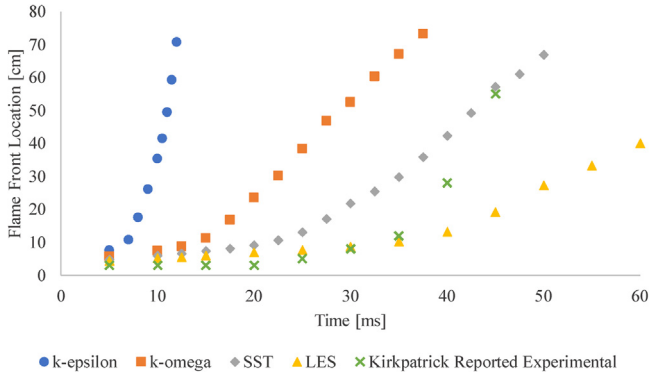

Fig. 13. Flame front location as a function of time for various turbulence models in 2D with the square obstacle. Temperature =293 K, Pressure = 101 kPa, E_{ign} = 60 mJ, Spark duration =1 ms.

was negligible change. This shows that flame stretching is likely occurring behind the obstacle due to the eddies formed in the wake. As the flame thickness decreases, the Karlovitz number, a dimensionless stretch factor, increases (Kuo and Acharya, 2012). Wrinkled laminar flames have a flame thickness that is smaller than the Kolmogorov microscale. The distributed reaction regime has flames with flame thicknesses larger than the integral length scale. Between the two regimes is the flamelets-in-eddies region. In the wrinkled laminar regime, the reaction regime, which occurs in thin sheets, is characterized by fast chemistry. The flamelets-in-eddies regime has high turbulence intensities and moderate Damköhler numbers. This regime has pockets of both burned and unburned gases in the flame zone (Turns, 2012). Damköhler has pointed out that the turbulent combustion regime is primarily classified by the scale of the turbulence compared to the flame thickness (Gülder, 1991). Flame thickness can then be used to determine behavioral characteristics of the flame and the interaction with turbulence.

Fig. 13 compares the results of the 2D model with the square obstacle for various turbulence models in addition to experimental results reported Kirkpatrick et al. (2003) (Kirkpatrick et al., 2003). Since results by Kirkpatrick et al. used a 79 mm square, the square of the 2D model was also changed to 79 mm for verification purposes. Flame front location of the experimental results was identified using photographs from a high-speed video camera operating at 400 frames per second in the experiment. With an average flame propagation velocity of 30 m/s after the flame passes the obstacle, the flame front location error is calculated as +/-3.75 cm for the experimental values.

The k-ε turbulence model extremely over predicted the flame propagation, propagating 4 times as fast as the experimental results

Table 7
Average flame propagation velocity after the flame impinges on the obstacle for five different spark location cases.

Spark Location Above Bottom [cm]	Flame Propagation Velocity [m/s]
0.5	19.1
1.0	18.2
2.5	11.3
5.0	23.0

by Kirkpatrick et al. (2003), shown in Fig. 13. This makes the k-ε model less suitable for confined combustion through obstacles when using ANSYS Fluent (Kirkpatrick et al., 2003). Large differences between the k-ε model results and experimental data are most likely due to the model's inability to accurately capture near-wall effects. Even with an enhanced wall treatment enabled, the model still produced the same over predicted propagation results. Capturing boundary layers formed by walls is important to accurately simulate the effect of obstacles on a flame, favoring a model that can capture shearing of the fluid.

In addition to accuracy, a short simulation time is also desired when determining requirements for a turbulence model. To simulate 25 ms, the SST model took 40.5 h while the LES and kω both took 29.5 h, each with a primary body sizing of 0.5 mm. For the k- ω and SST models where mesh independence was reached at a larger mesh of 2 mm, the computational time decreased to 3.5 and 7 h, respectively, to simulate 25 ms. Each model was run on 8 cores and 64 GB of RAM. Since high computing power is now more accessible, the computational time of a higher accuracy model, like the LES, is not as large of a restraint. If larger models were to be made and computational time was of high priority, a simpler model such as the k- ω could be considered along with incorporating meshing techniques to minimize the number of cells as that also has a significant impact on the computational time.

4.3. *Effect of spark ignition location*

Previous experiments and modeling, including those by Masri et al. (2002) and Kirkpatrick et al. (2003), did not specify the exact location of the spark ignition, simply stating that it was centered at the bottom of the chamber (Masri et al., 2000; Kirkpatrick et al., 2003). Depending on the spark ignition system used, the actual location of the flame kernel may vary by a few centimeters. A sensitivity analysis was done by varying the spark location to 0.5 cm, 1 cm, 2.5 cm, and 9.1 cm from the bottom of the chamber. Results presented thus far have all used a spark ignition location of 2.5 cm from the bottom of the chamber.

Fig. 14 shows that the further away an ignition occurs from an obstacle, the more unburnt gases there may be in front of the obstacle due to the stagnation pressure. This is especially apparent when the spark location is located at 0.5 cm from the bottom of the chamber where the layer of unburnt methane in front of the obstacle is 21 mm versus 4 mm when the spark is 5 cm from the bottom. Velocity streamlines also show some of the flow being pulled into vortices that form behind the obstacle while the flow downstream of the flame and further away from the obstacle is smoother. With the spark further away from the obstacle, the flame is able to spread in all directions, and by the time it approaches the obstacle, pressure has already built up in front of it, pushing the flame to the sides where there is less resistance. Fig. 15 shows flame propagation as a function of time for the varying spark location. Fig. 15 demonstrates that the flame propagation is highly dependent on where the spark location is. Table 7 shows the flame propagation velocity after the flame impinges on the obstacle for the five different spark location cases. These results show that to replicate the flame propagation after an ignition accurately, the spark location is critical. This

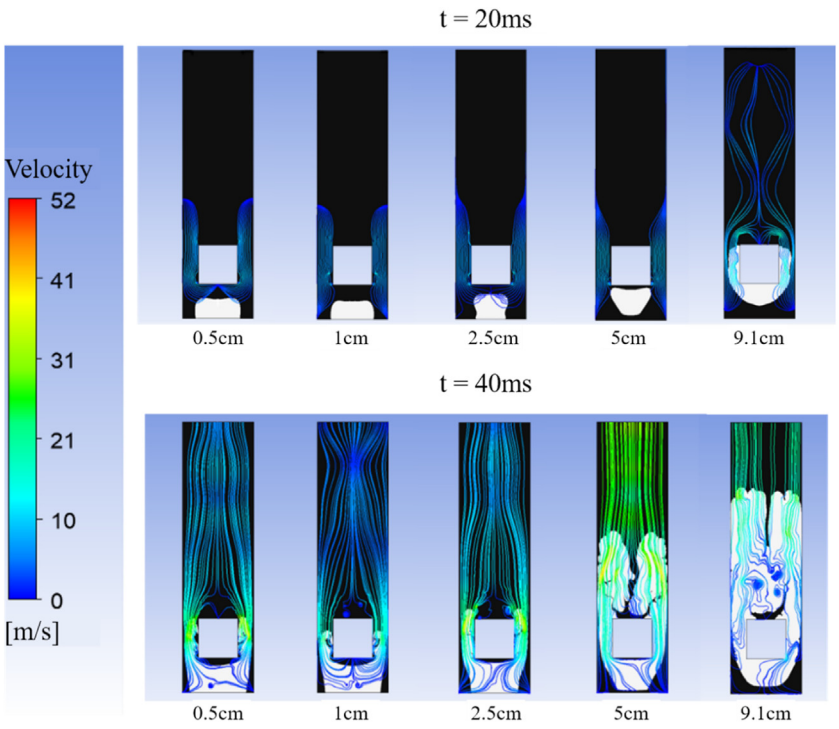

Fig. 14. Methane contour with velocity streamline overlay of 2D LES model at 20 and 40 ms with varying spark location. Values listed below each case is the vertical distance of the spark location from the bottom. Black contour represents unburnt methane while white contour represents products. Temperature =293 K, Pressure = 101 kPa, E_{ign} = 60 mJ, Spark duration =1 ms.

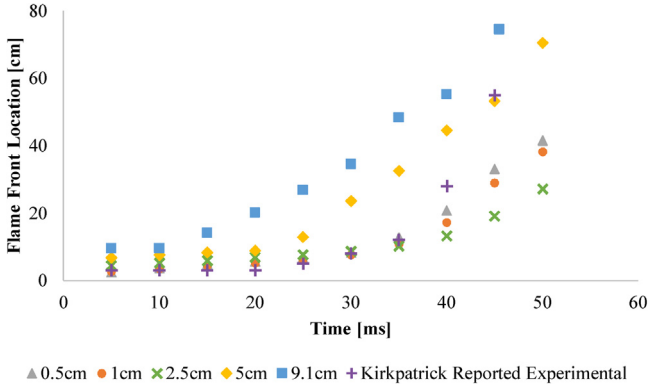

Fig. 15. Flame front location as a function of time of 2D LES model for varying spark locations with the square obstacle. Locations listed are the distance from the bottom of the chamber. Temperature =293 K, Pressure = 101 kPa, E_{ign} = 60 mJ, Spark duration =1 ms.

also underscores the importance of using a consistent spark plug or ignition device as the location where the spark actually occurs may vary on each device.

Having an obstacle in the flow introduces turbulence and thus the turbulent kinetic energy. Fig. 16 shows that when the ignition location is closer to the obstacle, there will be an increase in turbulent kinetic energy as the flame is able to interact with the obstacle faster. As the temperature increases during combustion, the diffusion will also increase, leading to a smaller Lewis number and thus an increase in turbulent kinetic energy (Chakraborty et al., 2011). It was also seen in the model by Chakraborty et al. (2011) that higher pressure gradients and pressure dilation help to counteract the decay of turbulent kinetic energy at Lewis numbers less than 0.8 (Chakraborty et al., 2011). Since the current model shows that mass diffusion may be greater than thermal diffusions, the current assumption of a Lewis at unity may not be appropriate to resolve highly turbulent flows. To address this, future work will include exploring turbulence-chemistry interaction.

4.4. Conclusion and future work

Testing flame propagation in methane-air mixtures past three shapes, a circle, a hexagon, and a square in a 2D model, shows that the shape of the obstacle impacts the flame propagation, with the square causing the fastest propagation. The sensitivity of flame propagation from the obstacle shape is also dependent on the turbulence model selected. When using an LES model, flame propagation is more sensitive to the shape of the obstacle than using a k-ω model.

From the four turbulence models tested, it can be concluded that the Large Eddy Simulation (LES) turbulence model is the most appropriate for situations where high turbulence and flame wrinkling is expected. Out of the four models, the LES accurately captured flame wrinkling on the flame front while maintaining reasonable simulation times. Even though the k-ε model had the fastest computational time, it over predicted how fast the flame would propagate.

Modeling results indicate that variation of the spark location by as small as 1 cm, which for this case corresponds to 10 % of the obstacle diameter, can result in a difference of the flame propagation. Increasing the distance between the obstacle and the ignition location resulted in a larger layer of unburnt methane in front of the obstacle.

Since the flow around the obstacles examined here was highly turbulent, researchers will further investigate turbulence-chemistry interaction. To capture the full effect of turbulence, future models will be brought into a three-dimensional model. Using a coarser grid with an adaptive mesh on a variable gradient is a possible method of limiting the necessary number of cells while also being able to capture the flame front. Temperature is not a fully accurate way to represent the flame front in this situation as

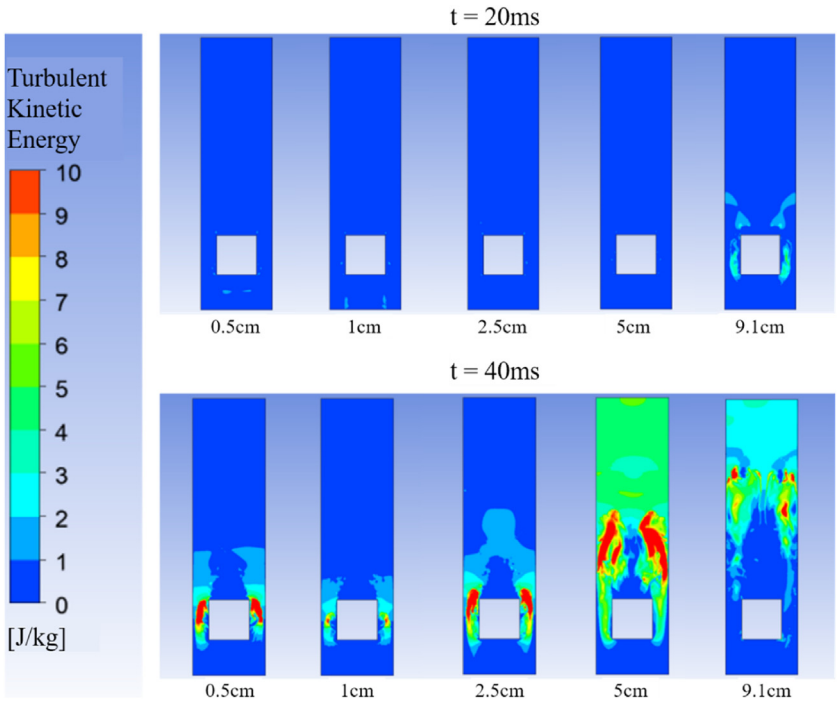

Fig. 16. Turbulent kinetic energy contour of 2D LES model at 20 and 40 ms with varying spark location. Temperature =293 K, Pressure = 101 kPa, E_{ign} = 60 mJ, Spark duration =1 ms.

the temperature diffused in large areas due to high turbulence, so other variables for gradient adaption should be tested. Tracking the OH radical would be a more accurate way of locating the flame front since the radical only exists in the reaction region; presence of the OH radical will require the number of steps used in the methane-air reaction to be increased, increasing computational time.

By strategically determining a turbulence model to best model turbulent flows in combustion, computational time can be reduced while still producing reliable results. Adaptive meshing methods will decrease the computational time, allowing researchers to solve larger and more complex problems. Findings from this research can be applied to a 3D model and give insight on turbulence model and obstacle shape selection.

Declaration of Competing Interest

The authors declare that they have no known competing financial interests or personal relationships that could have appeared to influence the work reported in this paper.

Acknowledgements

The work described in this paper was made possible with the support of the National Institute for Occupational Safety and Health (NIOSH) Contract # HCCR-2019-36403. This research was performed using the supercomputer Mio at the Colorado School of Mines.

References

ANSYS, Inc, 2013. ANSYS Fluent Theory Guide, 15th ed.
Argyropoulos, C., Markatos, N., 2015. Recent advances on the numerical modelling of turbulent flows. Appl. Math. Model. 39 (2), 693–732, http://dx.doi.org/10.1016/j.apm.2014.07.001.
Bailly, C., Comte-Bellot, G., 2015. Turbulence, 2nd ed. Springer International Publishing.
Barrett, E., 2019. China Factory Explosion That's Killed 78 Adds to Industrial Sector's Dark History of Deadly Accidents. Fortune.
Boger, M., Veynante, D., Boughanem, H., Trouvé, A., 1998. Direct numerical simulation analysis of flame surface density concept for large eddy simulation of turbulent premixed combustion. Symposium (International) On Combustion 27 (1), 917–925, http://dx.doi.org/10.1016/s0082-0784(98)80489-x.
Bray, K., Domingo, P., Vervisch, L., 2005. Role of the progress variable in models for partially premixed turbulent combustion. Combust. Flame 141 (4), 431–437, http://dx.doi.org/10.1016/j.combustflame.2005.01.017.
Brune, J., 2014. The methane-air explosion hazard within coal mine gobs. Mining Engineering Magazine (7).
Brune, J., Saki, S., 2017. Prevention of gob ignitions and explosions in longwall mining using dynamic seals. Int. J. Min. Sci. Technol. 27 (6), 999–1003, http://dx.doi.org/10.1016/j.ijmst.2017.06.026.
Chakraborty, N., Katragadda, M., Cant, R., 2011. Effects of Lewis number on turbulent kinetic energy transport in premixed flames. Phys. Fluids 23 (7), 075109, http://dx.doi.org/10.1063/1.3609278.
Chambers, R., Eng, P., Sauve, T., Eng, P., 2013. Methane Gas in Hog Barns. Ontario Ministry of Agriculture, Food and Rural Affairs.
Chen, P., Li, Y., Huang, F., Guo, S., Liu, X., 2016. Experimental and LES investigation of premixed methane/air flame propagating in a chamber for three obstacle BR configurations. J. Loss Prev. Process Ind. 41, 48–54, http://dx.doi.org/10.1016/j.jlp.2016.02.020.
Cullen, D., 1990. The Public Inquiry Into the Piper alpha Disaster. Department of Energy (UK), London, UK.
de Goey, L., Plessing, T., Hermanns, R., Peters, N., 2005. Analysis of the flame thickness of turbulent flamelets in the thin reaction zones regime. Proceedings Of The Combustion Institute, 859–866, http://dx.doi.org/10.1016/j.proci.2004.08.016, 30(1).
Di Sarli, V., Di Benedetto, A., Russo, G., 2009. Using Large Eddy Simulation for understanding vented gas explosions in the presence of obstacles. J. Hazard. Mater. 169 (1–3), 435–442, http://dx.doi.org/10.1016/j.jhazmat.2009.03.115.
Dryer, F., Glassman, I., 1973. High-temperature oxidation of CO and CH4. Symposium (International) On Combustion, 987–1003, http://dx.doi.org/10.1016/s0082-0784(73)80090-6, 14(1).
Gülder, Ö, 1991. Turbulent premixed flame propagation models for different combustion regimes. Symposium (International) On Combustion, 743–750, http://dx.doi.org/10.1016/s0082-0784(06)80325-5, 23(1).
Hawkes, E., Sankaran, R., Sutherland, J., Chen, J., 2005. Direct numerical simulation of turbulent combustion: fundamental insights towards predictive models. J. Phys. Conf. Ser. 16, 65–79, http://dx.doi.org/10.1088/1742-6596/16/1/009.
Ibrahim, S., Gubba, S., Masri, A., Malalasekera, W., 2009. Calculations of explosion deflagrating flames using a dynamic flame surface density model. J. Loss Prev. Process Ind. 22 (3), 258–264, http://dx.doi.org/10.1016/j.jlp.2008.05.006.
Juganda, A., Brune, J., Bogin Jr., G., Lolon, S., 2017. CFD modeling of longwall tailgate ventilation condition. In: SME Annual Conference and Exhibition., Denver, CO.
Kindracki, J., Kobiera, A., Rarata, G., Wolanski, P., 2007. Influence of ignition position and obstacles on explosion development in methane–air mixture in closed vessels. J. Loss Prev. Process Ind. 20 (4–6), 551–561, http://dx.doi.org/10.1016/j.jlp.2007.05.010.

Kirkpatrick, M., Armfield, S., Masri, A., Ibrahim, S., 2003. Large eddy simulation of a propagating turbulent premixed flame. Flow, Turbulence And Combustion (Formerly Applied Scientific Research) 70 (1–4), 1–19, http://dx.doi.org/10.1023/b:appl.0000004912.87854.35.

Kuo, K., Acharya, R., 2012. Turbulent and Multiphase Combustion. Wiley.

Lafay, Y., Renou, B., Cabot, G., Boukhalfa, M., 2008. Experimental and numerical investigation of the effect of H2 enrichment on laminar methane–air flame thickness. Combust. Flame 153 (4), 540–561, http://dx.doi.org/10.1016/j.combustflame.2007.10.002.

Law, C., 1989. Dynamics of stretched flames. Symposium (International) On Combustion, 1381–1402, http://dx.doi.org/10.1016/s0082-0784(89)80149-3, 22(1).

Li, Y., Chen, P., Bi, M., Gao, W., 2017. Premixed methane/air flame propagating in an obstructed chamber with different BRs and spatial configurations. J. Loss Prev. Process Ind. 47, 66–71, http://dx.doi.org/10.1016/j.jlp.2017.02.030.

Li, R., Malalasekera, W., Ibrahim, S., Liu, B., 2018a. On the mechanism of pressure rise in vented explosions: a numerical study. Process. Saf. Environ. Prot. 117, 551–564, http://dx.doi.org/10.1016/j.psep.2018.05.026.

Li, Q., Ciccarelli, G., Sun, X., Lu, S., Wang, X., Zhang, Z., et al., 2018b. Flame propagation across a flexible obstacle in a square cross-section channel. Int. J. Hydrogen Energy 43 (36), 17480–17491, http://dx.doi.org/10.1016/j.ijhydene.2018.07.077.

Liley, S., 2013. The Case for Safety: The North Sea Piper Alpha Disaster. No. 6. NASA Safety Center.

Masri, A., Ibrahim, S., Nehzat, N., Green, A., 2000. Experimental study of premixed flame propagation over various solid obstructions. Exp. Therm. Fluid Sci. 21 (1–3), 109–116, http://dx.doi.org/10.1016/s0894-1777(99)00060-6.

Masri, A., AlHarbi, A., Meares, S., Ibrahim, S., 2012. A comparative study of turbulent premixed flames propagating past repeated obstacles. Ind. Eng. Chem. Res. 51 (22), 7690–7703, http://dx.doi.org/10.1021/ie201928g.

Mine Safety and Health Administration, 2010. Upper Big Branch Mine-South, Performance Coal Company Fatal Accident Report. Mine Safety and Health Administration.

Moen, I., Donato, M., Knystautas, R., Lee, J., 1980. Flame acceleration due to turbulence produced by obstacles. Combust. Flame 39 (1), 21–32, http://dx.doi.org/10.1016/0010-2180(80)90003-6.

Moen, I., Lee, J., Hjertager, B., Fuhre, K., Eckhoff, R., 1982. Pressure development due to turbulent flame propagation in large-scale methane air explosions. Combust. Flame 47, 31–52, http://dx.doi.org/10.1016/0010-2180(82)90087-6.

Moin, P., Mahesh, K., 1998. DIRECT NUMERICAL SIMULATION: a tool in turbulence research. Annu. Rev. Fluid Mech. 30 (1), 539–578, http://dx.doi.org/10.1146/annurev.fluid.30.1.539.

Na'inna, A., Phylaktou, H., Andrews, G., 2014. Effects of obstacle separation distance on gas explosions: the influence of obstacle blockage ratio. Procedia Eng. 84, 306–319, http://dx.doi.org/10.1016/j.proeng.2014.10.439.

Na'inna, A., Phylaktou, H., Andrews, G., 2017. Explosion flame acceleration over obstacles: effects of separation distance for a range of scales. Process. Saf. Environ. Prot. 107, 309–316.

Nicoud, F., Ducros, F., 1999. Flow. Turbulence And Combustion 62 (3), 183–200, http://dx.doi.org/10.1023/a:1009995426001.

Park, D., Green, A., Lee, Y., Chen, Y., 2007. Experimental studies on interactions between a freely propagating flame and single obstacles in a rectangular confinement. Combust. Flame 150 (1–2), 27–39, http://dx.doi.org/10.1016/j.combustflame.2007.04.005.

Prasad, R., Gore, J., 1999. An evaluation of flame surface density models for turbulent premixed jet flames. Combust. Flame 116 (1–2), 1–14, http://dx.doi.org/10.1016/s0010-2180(98)00046-7.

Ranga Dinesh, K., Jiang, X., Malalasekera, W., Odedra, A., 2013. Large eddy simulation of fuel variability and flame dynamics of hydrogen-enriched nonpremixed flames. Fuel Process. Technol. 107, 2–13, http://dx.doi.org/10.1016/j.fuproc.2012.07.019.

Shih, G., 2019. After China's Deadly Chemical Disaster, a Shattered Region Weighs Cost of the Rush to 'get Rich. The Washington Post.

The Occupational Safety and Health Administration, 2019. Fire Protection and Prevention. The Occupational Safety and Health Administration.

Turns, S., 2012. An Introduction to Combustion, 3rd ed. McGraw-Hill, New York.

Wang, G., Ren, T., Cook, C., 2014. Goaf frictional ignition and its control measures in underground coal mines. In: Progress In Mine Safety Science And Engineering II., pp. 451–459, http://dx.doi.org/10.1201/b16606-85.

Wen, X., Yu, M., Liu, Z., Sun, W., 2012. Large eddy simulation of methane–air deflagration in an obstructed chamber using different combustion models. J. Loss Prev. Process Ind. 25 (4), 730–738, http://dx.doi.org/10.1016/j.jlp.2012.04.008.

Yu, M., Zheng, K., Chu, T., 2016. Gas explosion flame propagation over various hollow-square obstacles. J. Nat. Gas Sci. Eng. 30, 221–227, http://dx.doi.org/10.1016/j.jngse.2016.02.009.

Zipf, R., Gamezo, V., Sapko, M., Marchewka, W., Mohamed, K., Oran, E., et al., 2013. Methane–air detonation experiments at NIOSH Lake Lynn Laboratory. J. Loss Prev. Process Ind. 26 (2), 295–301, http://dx.doi.org/10.1016/j.jlp.2011.05.003.